AIP Applied Physics Letters

Formation of Y2O3 interface layer in a YMnO3/Si ferroelectric gate structure

Jae Hyoung Choi, Jeong Yong Lee, and Yong Tae Kim

Citation: Appl. Phys. Lett. 77, 4028 (2000); doi: 10.1063/1.1332101
View online: http://dx.doi.org/10.1063/1.1332101
View Table of Contents: http://apl.aip.org/resource/1/APPLAB/v77/i24
Published by the American Institute of Physics.

Additional information on Appl. Phys. Lett.

Journal Homepage: http://apl.aip.org/
Journal Information: http://apl.aip.org/about/about_the_journal
Top downloads: http://apl.aip.org/features/most_downloaded
Information for Authors: http://apl.aip.org/authors

ADVERTISEMENT

Downloaded 18 Apr 2013 to 143.248.118.122. This article is copyrighted as indicated in the abstract. Reuse of AIP content is subject to the terms at: http://apl.aip.org/about/rights_and_permissions

Formation of Y_2O_3 interface layer in a $YMnO_3$/Si ferroelectric gate structure

Jae Hyoung Choi and Jeong Yong Lee[a)]
Department of Materials Science and Engineering, Korea Advanced Institute of Science and Technology, Taejon 305-701, Korea

Yong Tae Kim
Semiconductor Materials Laboratory, Korea Institute of Science and Technology, P.O. Box 131, Cheongryang, Seoul, Korea

(Received 29 February 2000; accepted for publication 12 October 2000)

During the crystallization of amorphous $YMnO_3$ thin film on Si (100) at 870 °C in a dry O_2 ambient, a nanoprecipitate layer was found between the $YMnO_3$ and the Si substrate. Lattice image processing as well as high-resolution transmission electron microscopy showed that the nanoprecipitate layer was a cubic Y_2O_3 phase. Also, it showed that a native oxide was consumed by the reaction with the Y atoms. This [111] Y_2O_3 layer exhibited a local epitaxial relationship to the c-axis oriented (0001) $YMnO_3$. The formation of Y_2O_3 phase and the consumption of native oxide at the $YMnO_3$/Si interface are due to the Y atom which is better than Mn in its ability to oxidize during heat treatment in O_2 ambient. © *2000 American Institute of Physics.*
[S0003-6951(00)04550-2]

The low dielectric constant in ferroelectric thin films has been known as an essential factor for metal-ferroelectric-silicon field effect transistor (MFSFET), which is a cell device in the nondestructive readout (NDRO) ferroelectric random access memory (FRAM).[1,2] If the ferroelectric thin film with high dielectric constant is used directly on Si for the ferroelectric gate, the applied voltage for the ferroelectric thin film decreases significantly. This is due to the existence of the unwanted native oxide with low dielectric constant. Moreover, several problems concerning the reliability of MFSFET, such as retention, fatigue, depolarization, and memory window, are strongly related to the ferroelectric thin film/Si interface. To improve these problems, ferroelectric thin films with low dielectric constant have been proposed as well as inserting an insulating buffer film between the ferroelectric thin film and Si.[3,4]

Among these ferroelectric thin films, $YMnO_3$ has a hexagonal structure with lattice parameters of $a = 0.614$ nm and $c = 1.140$ nm, and a single polarization direction along the c axis.[5] In particular $YMnO_3$ has a low dielectric constant of 20, which is much lower than those of $PbZr_xTi_{1-x}O_3$ (PZT), $Bi_{3.25}La_{0.75}Ti_3O_{12}$ (BLT), and $SrBi_2Ta_2O_9$ (SBT). Therefore, considerable efforts have been made to prepare c-axis oriented $YMnO_3$ films for the MFSFET[4,6] and to obtain ferroelectric memory effects at low temperatures.[1,7] However, although interface information on $YMnO_3$/Si structure is very important in examining electrical properties such as the memory window, the atomic structure of the $YMnO_3$/Si interface is not seen carefully with high-resolution transmission electron microscopy (HRTEM), lattice image processing, and Auger electron spectroscopy (AES).

In this study, $YMnO_3$ thin films were deposited on p-Si (100) substrate with rf sputtering by using a $YMnO_3$ single target (purity = 99.9%) mixed with Y_2O_3 and Mn_2O_3 at a ratio of 1:1. During the deposition in an Ar ambient, the rf power density and chamber pressure were fixed at 1.85 W/cm^2 and 5×10^{-3} Torr, respectively. The thickness of the amorphous $YMnO_3$ films was about 25 nm, and for crystallization, the samples were annealed at 870 °C for 1 h in an oxygen atmosphere. After the crystallization process, the atomic structure and composition of the $YMnO_3$/Si interface were examined by HRTEM and AES. High-resolution micrographs were obtained with a JEOL JEM 2000EX microscope with point resolution of 0.21 nm operating at 200 kV. The atomic image processing was performed using the SEMPER6 PLUS program, developed by Synoptics, Ltd. HRTEM images were compared with diffractograms using this image processing to confirm our observations.

Figure 1 shows a cross-sectional HRTEM micrograph of $YMnO_3$/Si. It was deposited at Ar ambient, and then annealed at 870 °C for 1 h in a dry O_2 ambient. This figure reveals three distinct regions. First, there is a bottom amorphous layer about 13.0 nm thick. Second, there is a polycrys-

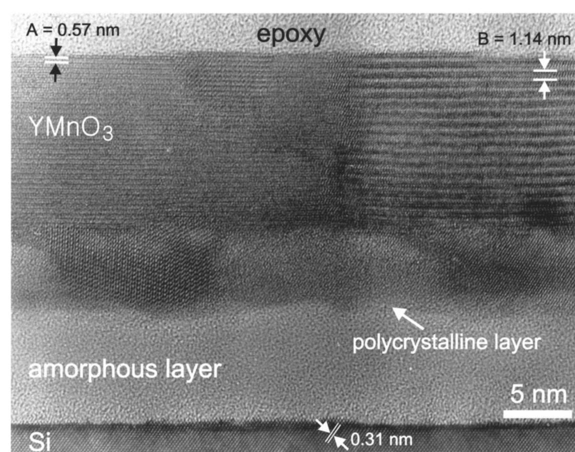

FIG. 1. Cross-sectional HRTEM micrograph of $YMnO_3$/Si deposited in Ar ambient and then annealed at 870 °C for 1 h in a dry O_2 ambient.

a)Electronic mail: jylee@mail.kaist.ac.kr

 © 2000 American Institute of Physics

Downloaded 18 Apr 2013 to 143.248.118.122. This article is copyrighted as indicated in the abstract. Reuse of AIP content is subject to the terms at: http://apl.aip.org/about/rights_and_permissions

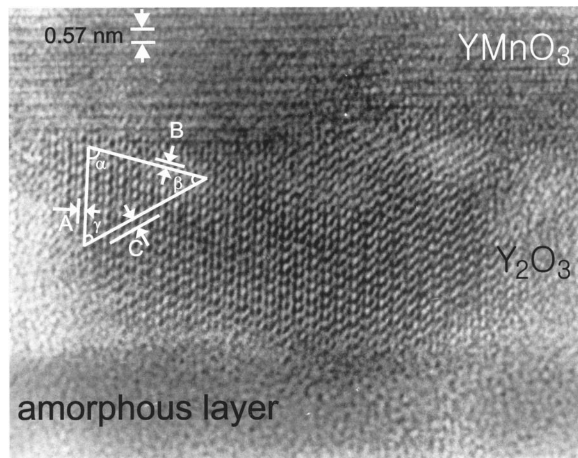

FIG. 2. Highly magnified HRTEM micrograph of the polycrystalline thin layer from Fig. 1.

talline layer about 8.5 nm thick. Third is a top layer of crystalline $YMnO_3$ about 20.0 nm thick. The distance between lattice planes, indicated by ''A'' and ''B'' in the $YMnO_3$ region, are 0.575 and 1.143 nm. These values are nearly the same as 0.570 and 1.140 nm which are the interplanar spacings of the (0002) and (0001) planes, respectively. It means that the c axes of $YMnO_3$ grains are preferentially oriented normal to the Si (001) surface. This figure also shows the interplanar distance between Si (111) planes, 0.314 nm, as a reference for the precise scale.

In order to analyze the polycrystalline thin layer more precisely, a middle section of Fig. 1 has been magnified, as shown in Fig. 2. In a triangle drawn in Fig. 2, the distance between lines indicated by ''A,'' ''B,'' and ''C'' are 0.306, 0.246, and 0.433 nm. These values are nearly the same as the spacings between the {311} planes, {133} planes, and {211} planes of the Y_2O_3 crystal, namely 0.311, 0.243, and 0.433 nm. These planes have a zone axis in the [011] direction, meaning that the Y_2O_3 grain is oriented in that direction as well. Furthermore, the angles between $(\bar{3}1\bar{1})$ and $(13\bar{3})$ planes, $(13\bar{3})$ and $(21\bar{1})$ planes, and $(21\bar{1})$ and $(\bar{3}1\bar{1})$ planes, which are indicated by ''α,'' ''β,'' and ''γ,'' are 77.5°, 42.5°, and 60°, respectively; these are very close to the theoretical values of 78.0°, 41.5°, and 60.5°. These lattice spacings and angles between planes indicate that the polycrystalline layer is matched with a cubic Y_2O_3 phase.

The diffractogram of the interface structure in Fig. 2 is presented in Fig. 3, together with a diagram identifying the diffraction spots. Reflections from both the $YMnO_3$ film and the Y_2O_3 precipitate can be clearly distinguished. The spacings between diffraction spots in Fig. 3 are inversely proportional to the spacings of lattice fringes in Fig. 2. It is apparent that the (0001) plane of $YMnO_3$ film is slightly deviated from the Y_2O_3 $[11\bar{1}]$ direction by the angle of 10°. In order to analyze the diffractogram quantitatively, the simulated atomic arrangements of (111) Y_2O_3 and (0001) $YMnO_3$ crystals are shown in Fig. 4. In the Y_2O_3 (111) surface, the distance (A_1) between adjacent Y atoms is 0.375 nm and the spacing (B_1) between Y rows is 0.325 nm. Figure 4(b) also shows that the spacing (A_2) between O atoms and the interplanar distance (B_2) between O rows in the $YMnO_3$ (0001) surface, are 0.354 and 0.307 nm, respectively. The ratios of

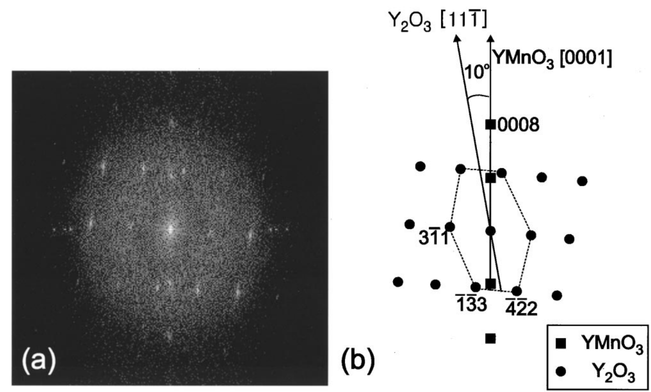

FIG. 3. (a) Computer-generated Fourier spectrum of the interface structure in Fig. 2 and (b) schematic representation.

A_1/B_1 and A_2/B_2 are equal to 1.06. Imada *et al.* have reported that (0001) $YMnO_3$ grows epitaxially on (111) Y_2O_3/Si structures by molecular beam epitaxy.[8] Thus it is very similar to the interface structure of molecular beam epitaxial $YMnO_3$ (0001) grown on Y_2O_3 (111) which was reported by Imada *et al.*

The formation of a polycrystalline Y_2O_3 layer at the $YMnO_3$/Si interface is caused by the difference in the oxidizing abilities of Y, Mn, and Si.[7] Also, as the Y/Mn ratio is larger than unity in the starting amorphous layer[4] it is natural to infer that Y species diffuse to the interface easily and are crystallized to Y_2O_3. The free energies for deoxidizing Y_2O_3, Mn_2O_3, $YMnO_3$, and SiO_2, which are thermodynamically calculated at 870 °C, are about 1558, 650, 1134, and 696 kJ/mol, respectively.[9,10] This means that the oxidizing ability of the Y atom is about 2.4 times greater than that of Mn. The easily oxidizing ability of the excess Y species produced the interface layer of the crystalline Y_2O_3 phase at the $YMnO_3$/Si interface. The most Mn species may not participate in the crystallization of Y_2O_3 and diffuse to $YMnO_3$ region. Thus, the composition of $YMnO_3$ film on the crystallized Y_2O_3 phase becomes more stoichiometric because ex-

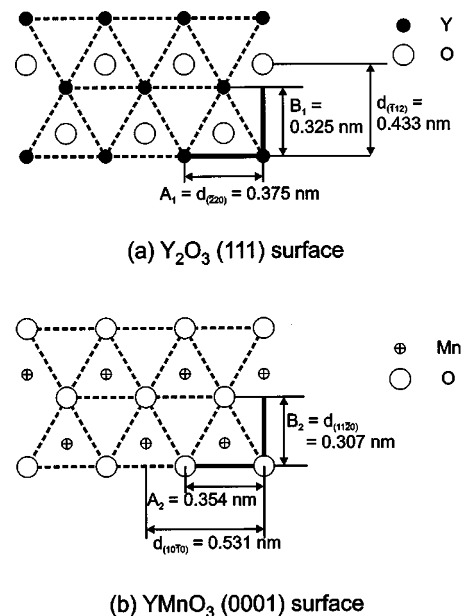

FIG. 4. Graphic representations of (a) Y_2O_3 (111) and (b) $YMnO_3$ (0001) surfaces.

Downloaded 18 Apr 2013 to 143.248.118.122. This article is copyrighted as indicated in the abstract. Reuse of AIP content is subject to the terms at: http://apl.aip.org/about/rights_and_permissions

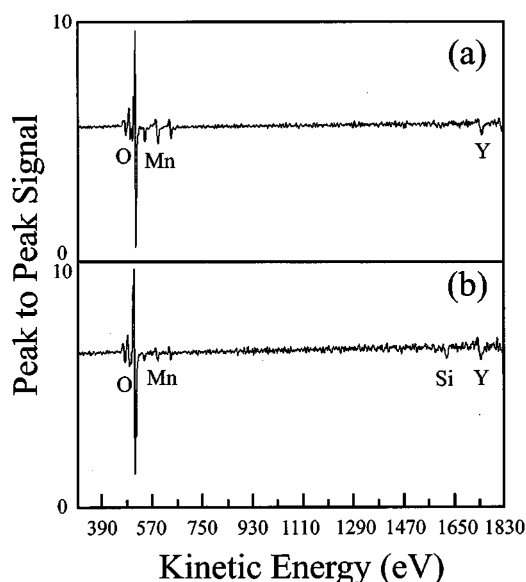

FIG. 5. AES signals from (a) polycrystalline region and (b) amorphous region in $YMnO_3$/Si interface.

cess Y species consumed by crystallization to Y_2O_3 phase at the interface. In the cubic Y_2O_3 structure, since the (111) plane would have the lowest surface energy, the (111) oriented Y_2O_3 can be easily obtained during the solid-phase crystallization. Thus, the c-axis-oriented $YMnO_3$ film can be grown on (111) Y_2O_3, taking account of the surface energy and epitaxial relationship between (0001) $YMnO_3$ and (111) Y_2O_3 during the crystallization.

In the amorphous region, the composition is somewhat complicated. Comparison of the cross-sectional HRTEM image of the as-deposited sample (not shown here) shows that the thickness of the amorphous layer increased from about 2 nm (native oxide) to 13 nm during heat treatment. If this amorphous layer is SiO_2, it is plausible that, since thermal oxide grows to about 15.0 nm during the dry oxidation of Si (100) wafers at 900 °C for 1 h,[11] the thickness of 13.0 nm is a natural result. However, AES signals for the polycrystalline layer [Fig. 5(a)] and amorphous layer [Fig. 5(b)] clearly show that the amorphous layer consists of Y as well as Si and O. Moving from the polycrystalline layer to the amorphous layer, the Mn concentration decreases whereas the Y concentration is rather constant, and a Si peak appears in the amorphous region. In particular, from the AES signals, the O concentration in the amorphous region is much smaller than that in the thermal oxide layer. During the solid-phase crystallization in a dry O_2 ambient, oxygen atoms can diffuse through the $YMnO_3$ film. These O atoms react with Y species to form crystalline Y_2O_3 phase because Y is one of the metals that have the highest affinity to oxygen.[12] Therefore, the further growth of SiO_2 is hindered by the formation of Y_2O_3. This formation of Y_2O_3 consumes the native oxide during the heat treatment, resulting in the Si-rich amorphous oxide at the Si side of the interface. This suggests that the amorphous layer is not a native oxide but rather a Si-rich Y–Si oxide. The driving force for reducing the SiO_2 might come from the crystallization of Y_2O_3 interfacial layer.

In conclusion, during the crystallization of amorphous $YMnO_3$ thin film on Si (001) at 870 °C in a dry O_2 ambient, a thin Y_2O_3 layer was formed at the $YMnO_3$/Si interface. High-resolution transmission electron microscopy and computer image processing revealed that the interplanar spacings and angles between different planes were clearly matched with those of cubic Y_2O_3. This polycrystalline Y_2O_3 layer had a local epitaxial relationship of $YMnO_3$ (0001)//Y_2O_3 (111). The formation of the Y_2O_3 layer and the consumption of SiO_2 in the amorphous layer are due to Y's high affinity to O during heat treatment in the O_2 atmosphere. This work suggests that, by depositing $YMnO_3$ thin film directly on Si for metal-ferroelectric-insulator-silicon FET (MFISFET), the separate preparation of an insulating buffer layer is not necessary. Moreover, the Y_2O_3 interfacial layer has relatively high dielectric constant ($\sim$15)[13] compared with SiO_2 (3.9) the layer might be the effect to increase the memory window and breakdown voltage and so on. Also this work may provide us the opportunity to fabricate self-formed ferroelectric/insulator/semiconductor gate structures by only controlling ferroelectric materials.

Further studies on the role of the nanoprecipitate Y_2O_3 layer in the electrical properties of c-axis oriented $YMnO_3$ films are in progress.

This study was supported by the Ministry of Science and Technology through a Project for National Research Laboratory in Korea and a Collaborative Project for Excellence in Basic System IC Technology (SYSTEM IC 2010).

[1] H. N. Lee, M. H. Lim, Y. T. Kim, T. S. Kalkur, and S. H. Choh, Jpn. J. Appl. Phys., Part 1 **37**, 1107 (1998).
[2] Y. T. Kim and D. S. Shin, Appl. Phys. Lett. **71**, 3507 (1997).
[3] W. C. Yi, J. S. Choe, C. R. Moon, S. I. Kwun, and J. G. Yoon, Appl. Phys. Lett. **73**, 903 (1998).
[4] H. N. Lee, Y. T. Kim, and Y. K. Park, Appl. Phys. Lett. **74**, 3887 (1999).
[5] H. L. Yakel, W. C. Koehler, E. F. Bertant, and E. F. Forrat, Acta Crystallogr. **16**, 957 (1963).
[6] N. Fujimura, T. Ishida, T. Yoshimura, and T. Ito, Appl. Phys. Lett. **69**, 1011 (1996).
[7] N. Fujimura, S. Azuma, N. Aoki, T. Yoshimura, and T. Ito, J. Appl. Phys. **80**, 7084 (1996).
[8] S. Imada, S. Shonriki, E. Tokumitsu, and H. Ishiwara, Jpn. J. Appl. Phys., Part 1 **37**, 6497 (1998).
[9] I. Barin, *Thermochemical Data of Pure Substances* (VCH, Weinheim, 1989), pp. 901, 1359, and 1675.
[10] H. Satoh, J. Iwasaki, K. Kawase, and N. Kamegashira, J. Alloys Compd. **268**, 42 (1998).
[11] O. D. Trapp, R. A. Blanchard, L. J. Lopp, and T. I. Kamins, *Semiconductor Technology Handbook* (Technology, San Mateo, CA, USA, 1982), p. 77.
[12] A. U. Seybolt and J. E. Burke, *Procedures in Experimental Metallurgy* (Wiley, New York, 1953), p. 176.
[13] A. Bardel, O. Eibl, T. Matthee, and J. Wecker, J. Mater. Res. **8**, 2112 (1993).

Downloaded 18 Apr 2013 to 143.248.118.122. This article is copyrighted as indicated in the abstract. Reuse of AIP content is subject to the terms at: http://apl.aip.org/about/rights_and_permissions